International Journal of ISSI, Vol. 12 (2015), No. 2, pp. 7-16

Growth Defects and Chromium Content Loss during the Deposition of Stainless Steel by CAE-PVD and Its Effect on the Corrosion and Passivation Behavior of the Coating

A. Sanati [1*], K. Raeissi [2], H. Edris [3]

[1, 2, 3] *Department of Materials Engineering, Isfahan University of Technology, Isfahan 84156- 83111, Iran*

Abstract

In the present study, the effects of growth defects and chromium content loss on the degradation of corrosion and passivation of cathodic arc evaporation (CAE-PVD) of stainless steel coating were investigated in 2 M sulphuric acid solution. EDS analysis indicated that the micro-particles were obtained during the coating growth. In addition, it was detected that the growth defects had poor adhesion to the coating matrix and in the open circuit potential (OCP), they were detached from the coating, providing appropriate conditions for the penetration of the solution. In addition, loss of chromium during evaporation was found to be detrimental to the passivation of the stainless steel coating and the formation of a porous oxide layer. The average percent of the main elements of the coating, according to EDS area analysis, was Fe-13Cr-6Ni. Moreover, the lower semicircle diameter of the coating in electrochemical impedance spectroscopy (EIS) measurements revealed the lower polarization resistance of it, in comparison to that of the bulk 304 stainless steel.

Keywords: Stainless steel coating, CAE-PVD, Growth defects, Corrosion, Passivation.

1. Introduction

Cathodic arc evaporation (CAE) is a physical vapor deposition (PVD) method with many advantages. Today, CAE-PVD has been widely used for common nitride coatings, such as TiN, TiAlN, AlCrN, and other hard coatings [1,2]. However, this method faces some obstacles in the evaporation of other materials such as aluminum and amorphous diamonds [2] and even some alloying materials. The major advantages of this process are the production of hard coatings with high density along with excellent adhesion to the substrate, high evaporation rate (among PVD methods), and full ionization of the plasma during deposition [3]. Indeed, an ionization ratio close to 100 % can be achieved through the CAE-PVD process, which is an advantage of this type of coatings [4]. In contrast to these features, the main disadvantage of this method is the production of coating defects such as macro-particles (macro-droplets) [2, 5] and other growth defects [6, 7]. Macro-particle generation is related to the formation of cathodic spot regions on the target and their contact with high pressure plasma during the deposition [2]. Other defects can be due to numerous factors. For example, improper pretreatments before coating deposition, such as grinding and polishing, can produce inclusions or defects on the coating surface [7, 8]. These growth defects influence many properties of the coating, such as optical features and corrosion behavior, and they can also increase surface roughness [6-8]. In addition, they have loose adhesion to the coating matrix and can be detached easily, thereby producing open routes to the substrate. They are known as pores or pinholes [9- 11].

In CAE-PVD processes, preventing the formation of these growth defects in the unfiltered condition is almost impossible. In a corrosive environment, aggressive anions (such as Cl^- or sulfide ions) can detach these defects from the coating and produce open ways to the substrate. Because of the nobler electrochemical nature of the coating, as compared to the substrate, this condition can build up galvanic cells which intensify the corrosion rate [12]. Furthermore, regarding iron substrate, it has been observed that the growth defects can decrease the corrosion potential of the coating to an amount close to that of the substrate by causing local corrosion and forming galvanic cells between the coating and the substrate [13].

Another issue regarding PVD evaporation methods is the difference in the compositions of target and coating, where alloying and multi-element systems have been applied. This difference results from the preferential evaporation of some elements (usually the elements with higher vapor pressure), causing the loss

* *Corresponding author*
Email: alisanati92@gmail.com
Address: Department of Materials Engineering, Isfahan University of Technology, Isfahan 84156- 83111, Iran.
1. PhD Student
2. Associate Professor
3. Professor

of other elements in the composition [14].

It seems that growth defects and loss of composition during the evaporation are the major parameters affecting the corrosion behavior of stainless steel coatings. In the present investigation, the effects of growth defects and chromium content loss on the corrosion and passivation of stainless steel coating produced by the unfiltered CAE-PVD method were studied.

2. Materials and Methods

2.1. Specimen preparation and deposition

The materials used as the target and the substrate, and the coating parameters are listed in Tables 1 and 2, respectively. Before the coating process, the substrates were wet ground up to #1500 grit using silicon carbide sandpaper (SiC); then they were polished using 0.05 microns Al_2O_3 powder. Finally, they were ultrasonically cleaned in sequences with acetone and ethanol solutions.

Just before the deposition, sputter cleaning of samples was performed by argon flow for 60 min in the PVD chamber. The deposition was conducted by a PVD system (model: Platit 2000) at Sevin Plasma Surface Engineering Company.

Fig. 1 shows a schematic illustration of the PVD system used. As can be seen, argon or nitrogen could be introduced from the top of the chamber to facilitate the deposition process. The vacuum pumps were situated at the bottom of the chamber and a stainless steel cathode was subjected perpendicular to the substrate surface with a distance of about 30 cm. The substrate was mounted on a rotating holder with a relative rotational speed of 6 rpm. Additional information is illustrated in Table 2.

Table 1. Composition of target and substrate (wt. %).

Sample	Fe	C	Si	P	S	Mn	Ni	Cr	Mo	Cu	Ti	V	Nb	Al
SS 304 (target)	69.270	0.087	0.246	<0.007	<0.030	1.400	10.600	17.500	0.098	0.329	0.354	0.038	0.048	-
Substrate	98.760	0.377	0.148	<0.008	0.164	0.524	<0.030	0.039	<0.008	0.067	0.010	<0.003	-	<0.008

Table 2. Applied deposition parameters for the stainless steel coating.

Parameter	Value
Vacuum pressure before deposition	10^{-5} Pa
Vacuum pressure during deposition	10^{-3} Pa
Target to substrate distance	30 cm
Applied current to target	110 A
Applied voltage to target	30 V
Substrate temperature	350 ºC
Substrate bias voltage	-300 V

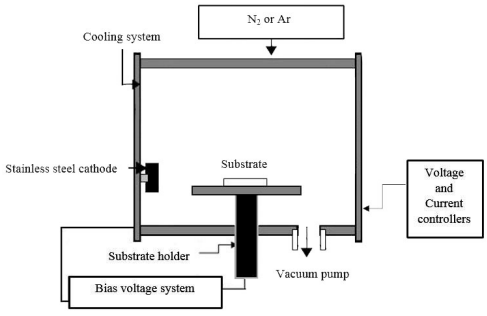

Fig. 1. A schematic illustration of the used PVD system.

2.2. Specimen characterization

X-ray diffraction (XRD) analysis was performed using a Philips X'Pert-MPD and the patterns were measured using Cu K_α radiation. The analysis was conducted at the range of $30° \leq 2\theta \leq 100°$. For XRD analysis, the coating was detached from an aluminum substrate and examined. To determine the peaks, X'Pert HighScore 2003 software was used. The cross-sectional and microstructural observations of as-deposited specimens and composition investigation were conducted using scanning electron microscope

(model: Philips XL30 SEM) and field emission scanning electron microscope (FE-SEM) equipped with an energy-dispersive X-ray spectroscopy (EDS) detector (model: Mira 3-XMU). The incident beam diameter for EDS analysis was about 80 nm. Stainless steel coating roughness was measured using a portable surface roughness tester (model: Serftest-SJ-210).

2.3. Corrosion and passivation measurements

Polarization and electrochemical impedance spectroscopy (EIS) measurements were carried out using an AMETEK advanced electrochemical system (model: PARSTAT 2273). A three electrode cell kit containing Ag/AgCl saturated with KCl as the reference electrode, Pt as the counter electrode, and the coated sample as the working electrode was applied. The corrosive solution was 2 M sulphuric acid. The working electrode had a surface area of 1 cm^2 and the distance between the reference and working electrodes was about 1 cm. In order to perform potentiodynamic tests, the samples were subjected to open circuit conditions until a steady-state potential was reached and the tests were performed with a scan rate of 1 mV/s at 25 ºC. EIS measurements were conducted using a frequency range of 100 kHz to 10 mHz with the potential amplitude of 10 mV. Before EIS measurements, the samples were maintained at 0.6 V versus Ag/AgCl for 1 h in order to form the passive layer. The EIS measurements were initiated immediately after the formation of the passive layer. All corrosion measurements were performed three times and the average values were reported. The EIS data were modeled by the Zview 2 software.

3. Results and Discussion

3.1. XRD analysis

Figs. 2a-c show the XRD results of stainless steel coating, carbon steel substrate, and bulk 304 stainless steel used as the target, respectively. It was evident that although the target had an austenitic structure (Fig. 2c), the stainless steel coating (Fig. 2a) was a two-phase material showing ferrite and very low-intensity austenite peaks. This condition can influence the corrosion behavior of the coating by building up a galvanic cell between these two phases. Austenitic sites can act as cathodic versus ferritic sites which are the anodic parts of the galvanic cell. The coating phase structure can be related to deposition parameters including target power, substrate temperature, and deposition rate [15]. However, in previous works on the deposition of stainless steels through PVD methods using the 304 stainless steel as a target, usually a complete ferritic structure has been reported [16,17]. Deviation of coating peak positions from those of the target could be due to changing of the crystalline lattice parameter. The deposition parameters can also be effective on the coating grain size and morphology [18].

Fig. 2a shows that the count number of coating was extremely decreased and the peaks were wider than those of the bulk 304 stainless steel. This was probably due to the lower grain size obtained for the stainless steel coating.

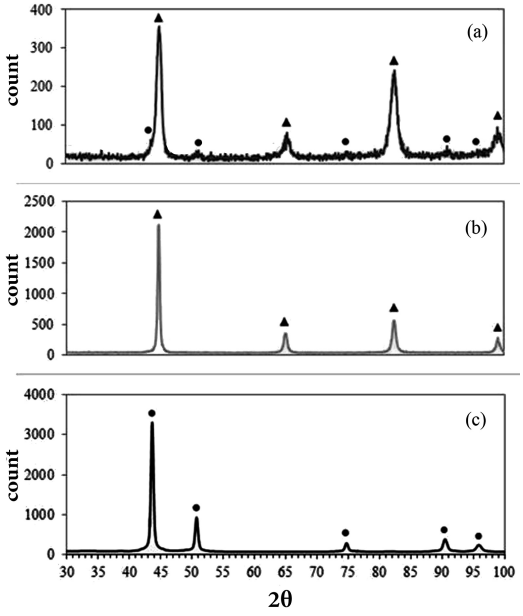

Fig. 2. XRD patterns of (a) the stainless steel coating, (b) the carbon steel substrate, and (c) the bulk 304 stainless steel used as the target. ▲Ferrite, ●Austenite.

3. 2. Surface morphology, EDS analysis, and coating cross-section

Fig. 3 shows the surface morphology of stainless steel coating. It was obvious that the coating surface was very rough. The spherical and needle-like particles were in the range of 1- 5 μm . Furthermore, there was no evidence showing pin holes or pores on the coating surface and the coating matrix was quite condensed. EDS spot analysis results were obtained from three separate locations on the coating surface. These locations are labeled in Fig. 3 by A, B, and C. Furthermore, a sample analysis was performed by EDS area analysis on the specified areas of the coating surface. It could be seen that no clear composition difference was found between these three locations. This confirmed that the particles rose during the coating growth. Thus, the difference observed between the composition of stainless steel coating and stainless steel target (evidently, the decrease of chromium content) occurred during the evaporation process. Because of the strength of the elements binding in such alloying systems, the evaporation of some elements

was very difficult; and thus some of the elements were not present in the coating during the deposition. Many parameters can determine the size and distribution of particles, but in the unfiltered CAE-PVD procedure, these particles have always been reported [2].

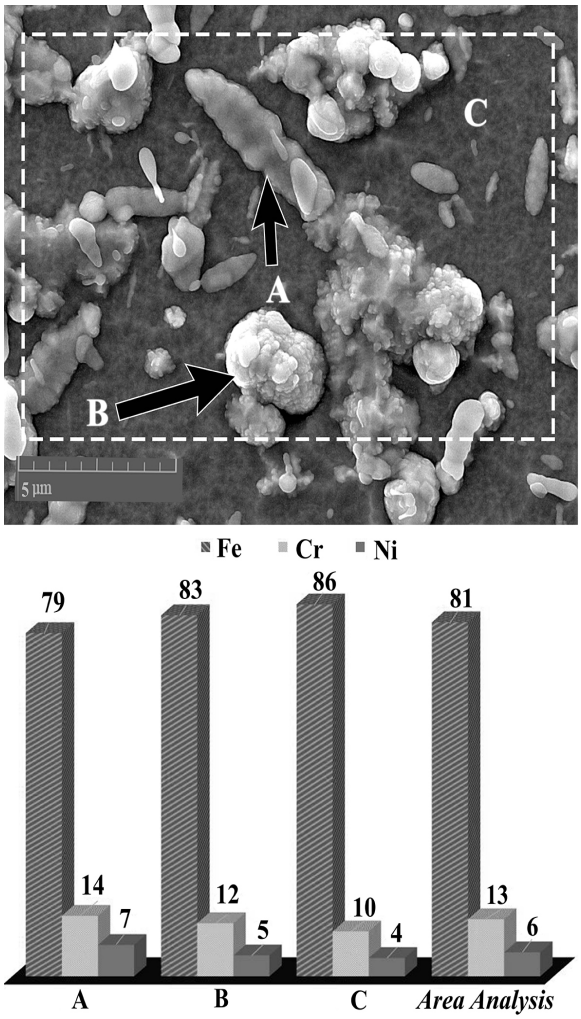

Fig. 3. FE-SEM image of the stainless steel coating surface and EDS results (wt.%).

Figs. 4a-d show the coating defects in cross-section views. In these Figs., ferrite-pearlite structure of the substrate and stainless steel coating thickness are visible. The average coating thickness of stainless steel was measured to be about 1.3 µm. Fig. 4 shows that near and/or beneath the surface particles, there were open pores which could provide easy paths for the aggressive solution to penetrate and reach the substrate. All these defects could increase the corrosion rate by building up galvanic corrosion cells (i.e. by forming local anodic and cathodic sites). Fig. 4a shows a large defect possibly grown on a substrate defect. Defects such as key holes were detected in stainless steel coating cross-section (Fig. 4b). The key holes are common defects inside the stainless steel coatings [8] which are not likely to influence the coating corrosion behavior. Fig. 4b also shows an open pore with no substrate contact resulting from the pull-out of one grown defect. Fig. 4c reveals an open channel reaching the substrate near one grown defect, and Fig. 4d shows a small defect with good adhesion to the substrate and the open channels near it.

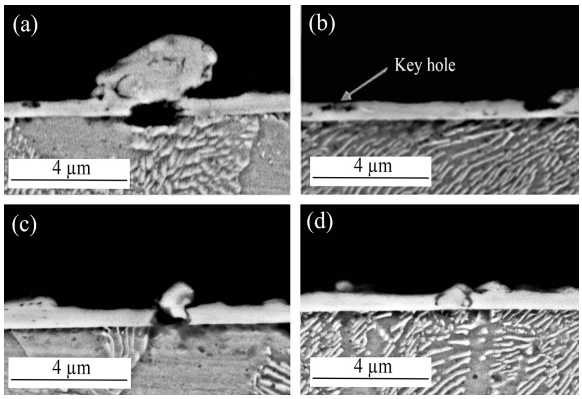

Fig. 4. BSE images of stainless steel coating cross-sections and the growth defects.

3.3. Corrosion behavior of the coating in 2 M sulphuric acid solution

3.3.1. OCP versus time readings

Fig. 5 shows the variation of open circuit potential (OCP) versus time for the bulk 304 stainless steel, the carbon steel substrate, and the stainless steel coating. The results showed that with increasing time, OCPs of bulk 304 stainless steel and the substrate were gradually increased during 1 h immersion.

Nevertheless, in the case of the coating, OCP varied in three stages; it could be seen that the OCP was raised for 20 min (I), but after this stage, it was decreased (region (II)) and at the final stage (region (III)), a steady state condition was reached. To evaluate this behavior, the samples were removed from the solution after 20, 40, and 60 min of immersion and their surfaces were examined using SEM. The results are presented in Fig. 5.

It was clear that, simultaneously, the coating matrix corrosion was initiated adjacent to the growth defects, propagating into the coating matrix with higher rates (Fig. 6a).

It could be clarified that with increasing the immersion time (Figs. 6b and c), the coating corrosion was intensified and surface roughness was decreased by the elimination of the growth defects. The dark regions near the growth defects in Fig. 6b indicated that the corrosion was in progress there. The area of these dark regions was also increased with time (Fig. 6c), and the matrix attacks at these defective sites were evidenced.

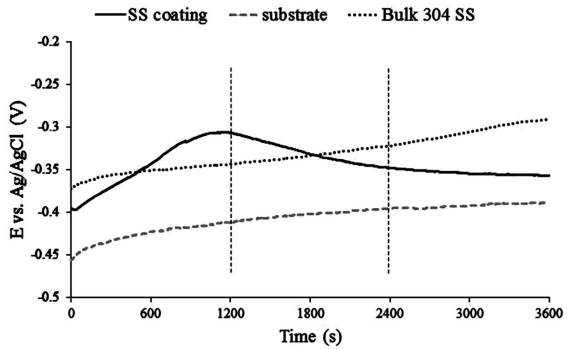

Fig. 5. OCP versus time readings for the bulk 304 stainless steel, the substrate, and the stainless steel coating in 2 M sulphuric acid solution.

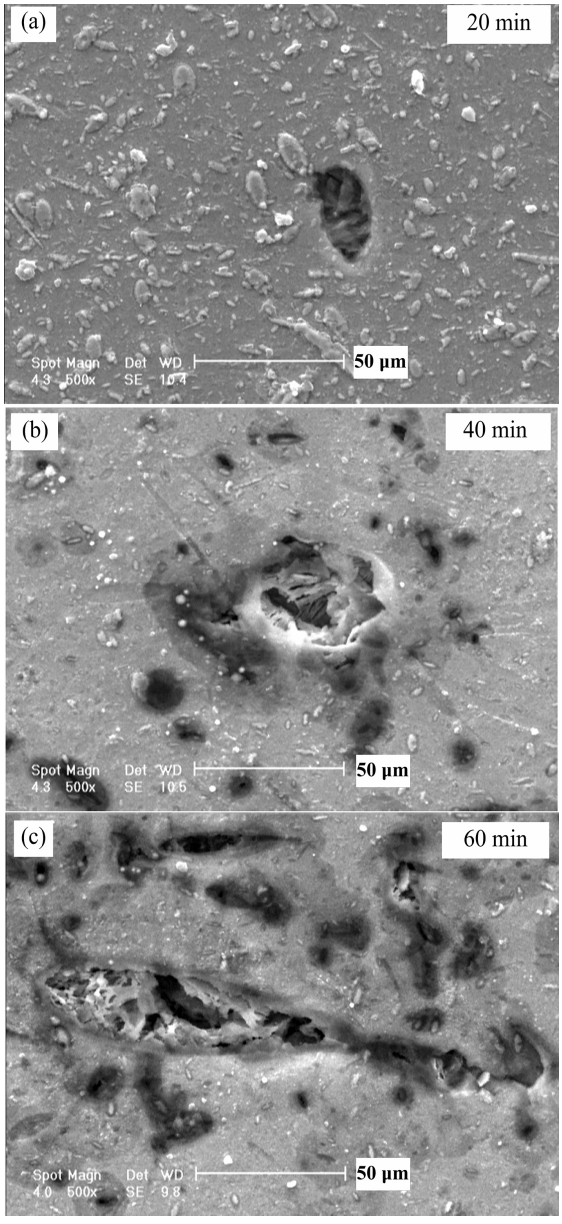

Fig. 6. Stainless steel coating corrosion observed at OCP after 20, 40, and 60 minutes of immersion in 2 M sulphuric acid solution.

3.3.2. Potentiodynamic polarization tests in 2 M sulphuric acid solution

In acidic solutions and at anodic potentials, selective dissolution of iron occurs, resulting in the chromium enrichment of the passive layer for iron-chromium alloys [19]. This is the main reason for the passivation of iron-chromium alloys in acidic media. Fig. 7 and Table 3 show the results of potentiodynamic tests and the extracted corrosion parameters for the bulk 304 stainless steel, the substrate, and the stainless steel coating.

According to Table 3, it can be seen that the corrosion current density of coating (0.0008961 A cm^{-2}) was extremely higher than that of the bulk 304 stainless steel (0.0000108 A cm^{-2}) and the substrate (0.0004854 A cm^{-2}). This was because the coating defects increased the corrosion rate. However, the corrosion potential of the coating was higher than that of the substrate. This could arise from the chromium present in the composition of the coating. Nevertheless, the primary passivation potential (E_{pp}) of the stainless steel coating was about 0.4 Vdc. This was because chromium content loss occurred during deposition [20]. In the potential range of 0.1- 0.33 Vdc, the stainless steel coating behaved in a way similar to the substrate. This is known as the region of iron sulfide formation [21]. Indeed, with increasing the potential beyond this region, the current density was decreased, but the current density was very high, depicting a defective oxide layer. However, the transpassive potential of the coating was 1 Vdc, while this parameter for the bulk 304 stainless steel was about 0.85 Vdc. It should be noted that the transpassivation for the stainless steel in sulphuric acid solutions arises from dissolving chromium, iron, and nickel as Cr^{6+}, Fe^{3+}, and Ni^{2+}, respectively [22]. Furthermore, for voltages over 1.4 Vdc, the coating behaves like the substrate, where the coating is detached. The main effect of nickel on potentiodynamic curves is on i_{crit}, where the presence of nickel decreases the required current density for active/passive transition [22]. This effect can be clearly seen in Fig. 7 for the stainless steel coating with respect to the substrate. In normal conditions, the chromium percentage in the passive layer is about 50-70 %, and by increasing the potential, iron percentage is increased [19].

In the passive range of the stainless steel coating, since iron can form Fe_2O_3 layer and there are growth defects and open paths to the substrate, probably, iron can be easily diffused in the passive layer and its fraction in the passive layer exceeds the normal level. This passive layer provides no acceptable protective properties.

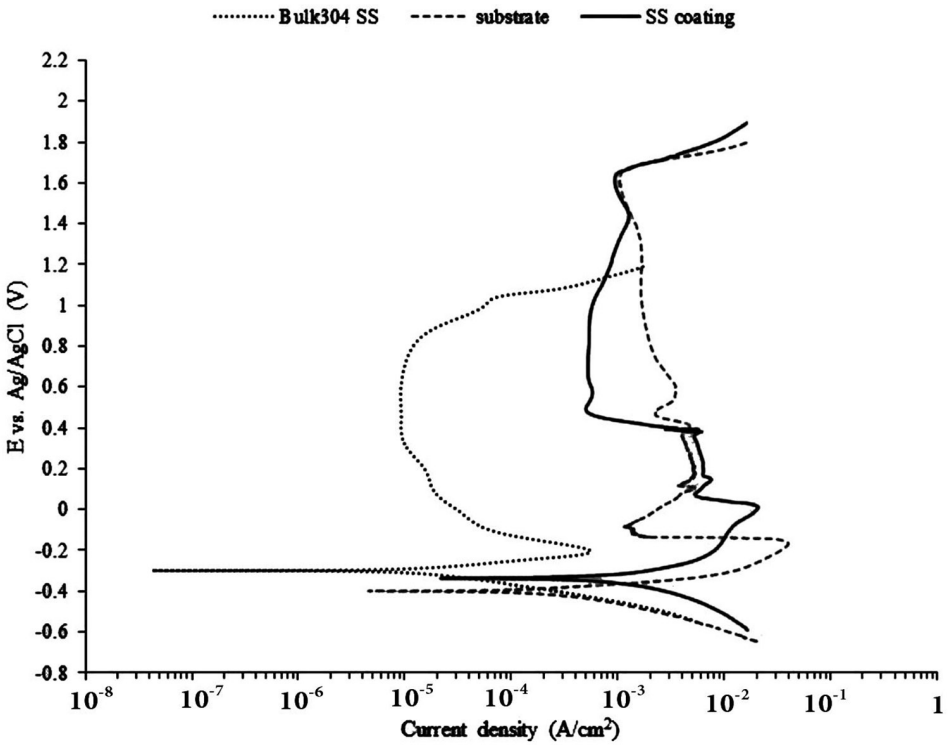

Fig. 7. Potentiodynamic curves in 2 M sulphuric acid.

Table 3. Corrosion parameters extracted from potentiodynamic plots in Fig. 7.

Sample	E_{corr} (V)	i_{corr} (A/cm^2)	R_p (Ω.cm^2)	β_a (V/dec)	β_c (V/dec)
SS coating	-0.3599	0.0008961	19.44	0.078	-0.082
Substrate	-0.3987	0.0004854	33.52	0.064	-0.090
Bulk 304 SS	-0.3020	0.0000108	1131	0.049	-0.067

3.3.3. Potentiostatic tests in 2 M sulphuric acid solution

In order to evaluate the passive behavior of the stainless steel coating, potentiostatic measurements were conducted at 0.2 and 0.6 V for 1 h. The results are illustrated in Fig. 8. It could be seen that for both potentials, current density was decreased after applying the potential. However, at 0.2 V, it was increased after decaying. At 0.6 V, the current density remained constant with the increase of time, thereby indicating passivation. However, a more detailed study of the variation of current density at this potential (inserted Fig. 8) showed an increase of current density in a very small scale. This showed that the oxide layer developed on coating could not be considered as a perfect passive layer (barrier layer), because, as mentioned before, it was very deficient.

One of the methods used for detecting the passive behavior is drawing potentiostat data using double logarithmic curves, where the logarithm of current density is plotted versus logarithm of time. Therefore, the current density is decreased with time according to the following equation [23, 24]:

$$i = 10^{-(A + k \log t)} \qquad \text{Eq. (1)}$$

, where k reveals the slope of the double log curve. When k = -1, a compact and high protective oxide layer is expected, while k = -0.5 represents a porous and defective oxide layer [23, 24]. The double log curves for the bulk 304 stainless steel and the stainless steel coating at 0.6 V are plotted in Figs. 9a and b, respectively. Extracting the slope of plots conducted by the linear trend line and R^2 evaluation showed deviation from the normal condition (where $R^2 = 1$).

Here, k = -0.7736 for the bulk 304 stainless steel and k = -0.6399 for the stainless steel coating specified that the oxide layer of the stainless steel coating was more defective than that of the bulk 304 stainless steel.

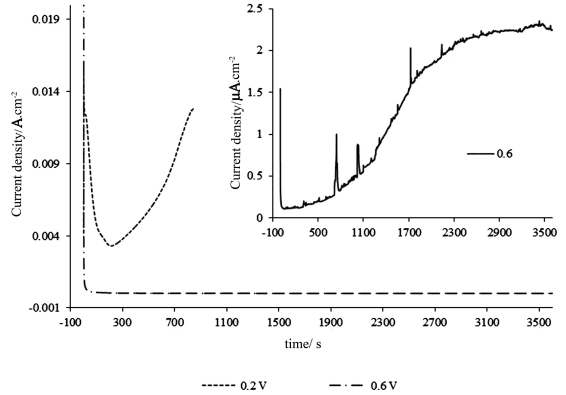

Fig. 8. Potentiostatic curves for determining the passivation behavior of stainless steel coating oxide layer.

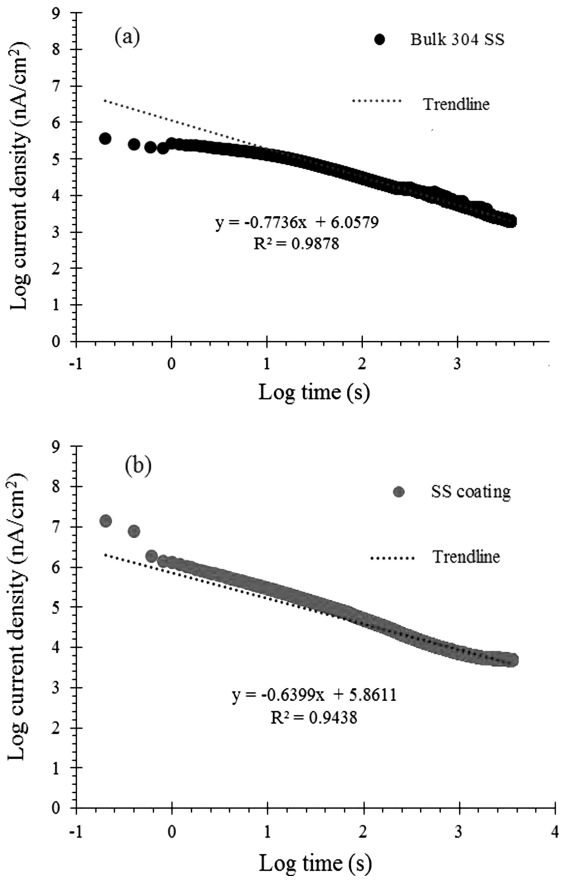

Fig. 9. Double log plot according to potentiostat tests at 0.6 V for the Bulk 304 stainless steel and the stainless steel coating.

3.3.4. EIS measurements in 2 M sulphuric acid solution

Figs. 10 and 11 show EIS and the simulated data of the bulk 304 stainless steel and the stainless steel coating after being at 0.6 V for 1 h. A semicircle capacitance loop for both samples has been evidenced in Nyquist plots (Fig. 10). The lower semicircle diameter of coating, rather than the bulk 304 stainless steel, depicted its lower polarization resistance. Moreover, according to Fig. 11a, at low frequencies, |Z| value for the stainless steel coating was lower than that of the bulk 304 stainless steel, thereby confirming this fact. In Bode-phase plots, the decrease in the phase value with moving in the opposite direction after a maximum phase peak shows the presence of a defective oxide layer [25].

The possibility of defect existence in the oxide layer for both samples has been previously shown using the results of double log plots (Fig. 9). The equivalent circuit (EC) model used for simulating the impedance data is described in detail in Fig. 11, where a bilayer model for passive behavior is suggested. This model has been proposed by Olefjord and Elfstorm for the passive corrosion of austenitic stainless steel in acidic solutions [26].

Accordingly, the passive layer consists of an oxy-hydroxide film as an outer layer rich in Fe^{3+} and an inner layer of a mixed oxide of iron-chromium-nickel [27- 29]. In addition, bilayer passive films can also be confirmed by PDM [30].

The passive layer is constructed from a highly defective barrier layer as the inner layer and the outer layer, which is formed by the transition of hydrolyzed cations through this barrier layer and the subsequent precipitation of hydroxide, oxy-hydroxide, or oxide. However, this is dependent upon the passive film formation condition. Therefore, the simulated data can be different in a range of potentials and acid concentrations.

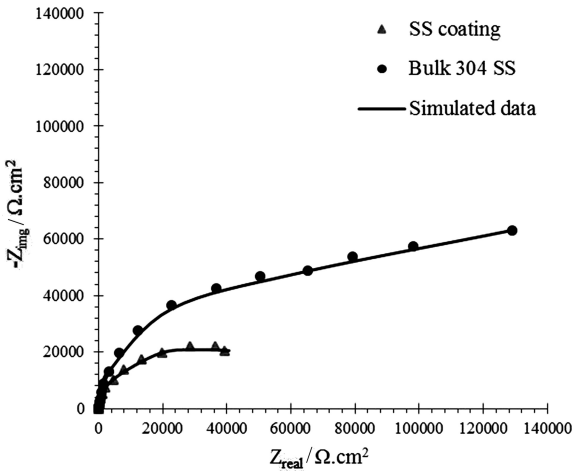

Fig. 10. Nyquist and simulated curves for the bulk 304 stainless steel and the stainless steel coating.

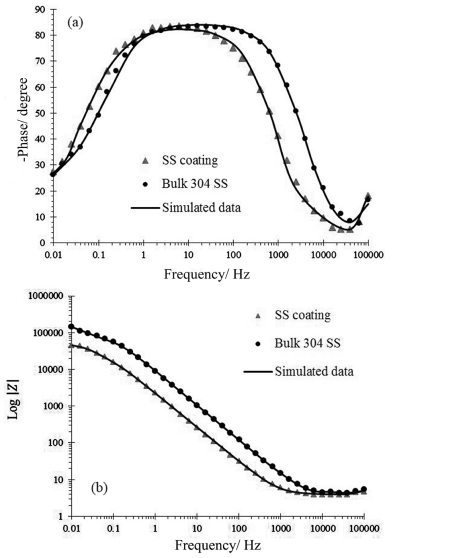

Fig. 11. Bode-Z curves and Bode phase curves and the corresponding simulated data for the bulk 304 stainless steel and the stainless steel coating.

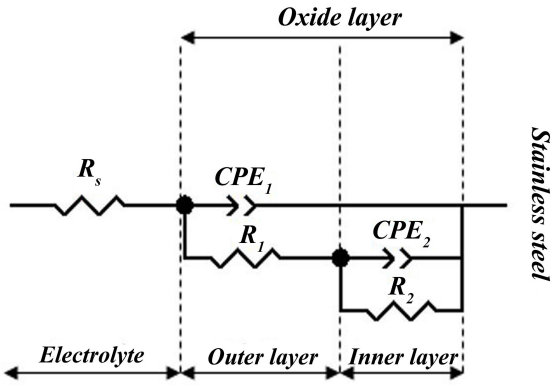

Fig. 12. The electrical circuit model used for simulating the passive corrosion of stainless steels.

Here, according to the simulated model (Fig. 12), R_1, CPE_1, R_2, and CPE_2 in EC series were resistances and capacitances of outer and inner oxide layers, respectively. Thus, the total polarization resistance (Rp) of the oxide layer was $R_1 + R_2$. The higher polarization resistance showed the better passivation behavior and it was inversely related to the corrosion rate [31, 32]:

CPE is a complex element frequently used in order to take into account the observed frequency dispersion. Z_{CPE} is defined as the impedance of CPE as follows [29, 31]:

$$Z_{CPE} = 1/Q(j\omega)^n \quad \text{Eq. (2)}$$

, where n depicts the degree of deviation from the pure capacitance. When n = 1, it means that CPE is equal to a pure capacitor, and Q defines CPE admittance [29, 31], in the range of 10^{-5} to 10^{-6} Ω^{-1} cm^{-2} s^n, thereby reflecting the formation of the passive layer [31,33].

In addition, ω is the angular frequency. The resistance at the high frequencies corresponds to R_s, which implies the solution resistance. Here, the mathematical expression of the passive layer impedance can be calculated as follows:

$$Z = R_s + (1/(1/R_1) + (Q_1(j\omega)^{n_1})) + (1/(1/R_2) + (Q_2(j\omega)^{n_2})) \quad \text{Eq. (3)}$$

The electrochemical parameters obtained by fitting the experimental data are listed in Table 4. If the outer layer were very porous, R_1 would correspond approximately to the resistance of the electrolyte inside the pores [25]. However, the simulated results depicted the formation of a partly compact outer layer in both cases. This situation has been previously reported in EIS simulated data for AISI 321 stainless steel in concentrations ≥ 0.1 M H_2SO_4 [34]. As can be seen in Table 4, the overall polarization resistance of the stainless steel coating was lower than that of the bulk 304 stainless steel, indicating the higher corrosion rate and the weaker nature of the oxide layer for the stainless steel coating.

The chromium content of the oxide layer can influence its capacitance value. Therefore, the lower content of chromium in the coating oxide film leads to the weaker passivation behavior (i.e. higher Q values than those of the bulk 304 stainless steel).

Table 4. Electrical elements obtained by fitting EIS results in Fig. 9 using the EC model described in Fig. 11.

Element	Bulk 304 stainless steel	Stainless steel coating
R_s (Ω.cm^2)	4.27	4.02
R_1 (Ω.cm^2)	88080	34540
Q_1 (Ω^{-1}cm^{-2}s^n)	1.91×10^{-5}	8.03×10^{-5}
n_1	0.94	0.93
R_2 (Ω.cm^2)	89824	42954
Q_2 (Ω^{-1}cm^{-2}s^n)	1.3×10^{-4}	1.8×10^{-4}
n_2	0.99	0.62

3.3.5. Corrosion mechanism in 2 M sulphuric acid solution

Fig. 13 shows the corroded coating surface after polarization reading, where the coating was detached from the substrate at high potentials. Corrosion products in local regions can be clearly seen in this Fig. Fig. 14 shows a schematic representing the

corrosion process model of the stainless steel coating for describing polarization behavior and features observed in Fig.13. Fig. 14a shows the cross-section of the stainless steel coating, and Fig. 14b displays the coating during OCP condition, where the growth defects and the coating matrix were corroded (as deduced from potentiodynamic results). However, corrosion attack in local sites near the growth defects (because of the chromium difference between the growth defect and its adjacent sites) was initiated with higher corrosion rates. Finally, in this stage, the pull-out of growth defects occurred where the steady state condition was reached. Fig. 14c shows the formation of a defective oxide layer in passive potentials. On the other hand, ions release of oxide layer in transpassive region is shown in Fig. 14d. Fig. 14e shows the progress of corrosion attack (dark sites), where stainless steel coating matrix and the resulting pores acted as cathode and anode, respectively. Therefore, galvanic cells built up between the stainless steel coating and the substrate could further increase the intensity of the corrosion; finally, the coating was detached from the substrate.

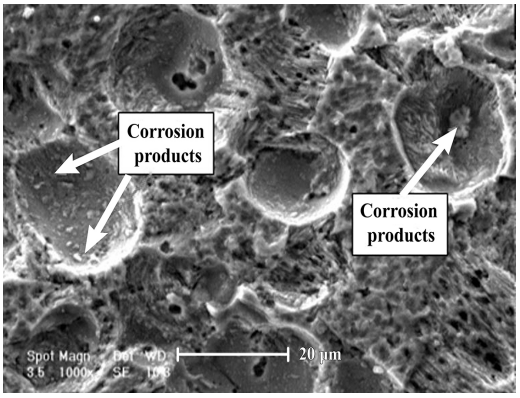

Fig. 13. Stainless steel coating surface at the end of polarization reading in 2 M sulphuric acid solution.

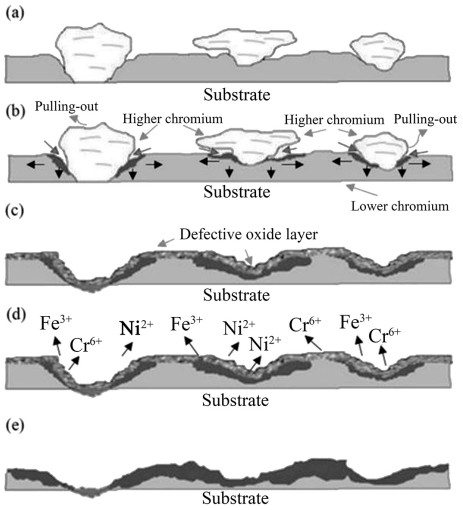

Fig. 14. Schematic illustration of the corrosion process for stainless steel coating in 2 M sulphuric acid.

4. Conclusions

According to the results of the conducted analysis, it was observed that the growth defects and the chromium content loss occurred during deposition by CAE-PVD, showing major effects on the degradation of corrosion and passivation of the stainless steel coating. It could be clarified that in the OCP condition, the coating corrosion was intensified and surface roughness was decreased by the elimination of the growth defects, thereby providing appropriate conditions for the penetration of solution. During the potentiodynamic measurements, the corrosion current density in the presence of growth defect was increased significantly by building up galvanic cells between the coating and the substrate. Moreover, the log-log and EIS results confirmed the formation of a defective oxide layer for the stainless steel coating. The proposed equivalent circuit for the stainless steel coating in acidic solution was a bilayer model with lower polarization resistance than that of the bulk 304 stainless steel.

Acknowledgements

The authors would like to thank the Sevin Plasma Surface Engineering Company in Isfahan, Iran, for providing the coating deposition facilities.

References

[1] M. Mühlbacher, R. Franz, J. Paulitsch, H. Rudigier, P. Polcik, P. H. Mayrhofer, C. Mitterer: Surf. Coat. Technol., 215 (2013), 96.
[2] A. Andre´: Surf. Coat. Technol., 120–121 (1999), 319.
[3] B. A. Saleh, I. Kenichi: Surf. Coat. Technol., 237(2013), 421.
[4] M. Darina, W. G. Jürgen, M. Stephan: Mater., 3(2010), 4109.
[5] S. G. Harris, E. D. Doyle, Y. C. Wong, P. R. Munroe, J. M. Cairney, J. M. Long: Surf. Coat. Technol., 183 (2004), 283.
[6] P.C. Panjan, M. Panjan, M. Kek-Merl, D. Kek-Merl: Vac., 84(2010), 209.
[7] P. Panjan, D. Kek-Merl, F. Zupanič, M. Čekada, M. Panjan: Surf. Coat. Technol., 202(2008), 2302.
[8] P. Panjan, P. Gselman, D. Kek-Merl, M. Čekada, M. Panjana, G. Dražić , T. Bončina, F. Zupanič: Surf. Coat. Technol., 237(2013), 349.
[9] H. W. Wang, M. M. Stack, S. B. Lyons, P. Hovsepian, W. D. Miinz: Surf. Coat. Technol., 126(2000), 279.
[10] S. H. Ahn, J. H. Lee, J. G. Kim, J. G. Han: Surf. Coat. Technol., 177 –178(2004), 638.
[11] C. B. Liu, Q. , A. Leyland, A. Matthews: Corros. Sci., 45(2003), 1243.
[12] H. Altun, S. Sen; Mater. Des., 27(2006), 1174.
[13] M. Li, S. Luo, C. Zeng, J. Shen, H. Lin, C. Cao: Corros. Sci., 46(2004), 1369.

[14] Y. Pauleau, P. B. Barna: 'Protective Coatings and Thin Films: Synthesis, Characterization and Applications', Kluwer academic publisher, Netherlands, (1996),
[15] P. Chen, L. Li, L. Ying, W. Shenggang, W. Fuhui: Electrochim. Acta., 56(2011), 7740.
[16] Y. S. Song, J. H. Lee, K. H. Lee, D. Y. Lee: Surf. Coat. Technol., 195(2005), 227.
[17] C. M. Fernandes, V. M. Ferreira, A. M. R. Senosa, M.T. Vieira: Surf. Coat. Technol., 176(2003), 103.
[18] A. André:, Thin Solid Films., 518(2010), 4087.
[19] C. O. A. Olsson, D. Landolt; Electrochim. Acta., 48(2003), 1093.
[20] C. A. Della Rovere, J.H. Alano, R. Silva, P.A.P. Nascente, J. Otubo, S.E. Kuri: Corros. Sci., 57(2012), 154.
[21] Z. Panossian, N. L. De Almeida , R. M. F. De Sousa, P. G. De Souza, L. B. S. Marques: Corros. Sci., 58(2012), 1.
[22] K. Osozawa, H. J. Engell: Corros. Sci., 6(1966), 389.
[23] Y. Wei, L. Ying, W. Fuhui: Electrochim. Acta., 51(2006), 4426.
[24] M. Lakatos-Varshyi, F. Falkenberg, I. Olefjord: Electrochim. Acta., 43(1998), 187.
[25] G. K. Robert, R. S. John, W. S. David, G. B. Rodulph: 'Electrochemical Techniques in Corrosion Science and Engineering', Marcel Dekker Inc, New York, (2002), 226.
[26] I. Olefjord, B. O. Elfstrom: Corros., 3(1982), 46.
[27] F. Gaben, B. Vuillemin, R. Oltra: J. Electrochem. Soc., 151(2004), B595
[28] N. E. Hakiki, M. D. Belo, A. M. P. Simoes, M. G. S. Ferreira: J. Electrochem. Soc.,145(1998), 3821.
[29] Y. X. Qiao, Y. G. Zheng, P. C. O. W. Ke: Corros. Sci., 51(2009), 979.
[30] D. D. Macdonald,: J. Electrochem. Soc., 153(2006), B 213.
[31] C. Escrivà-Cerdán, E. Blasco-Tamarit, D. M. García-García, J. García-Antón, A. Guenbour: Electrochim. Acta., 80(2012), 248.
[32] M. Metikoš-Hukovic´, R. Babic´, Z. Grubacˇ, Z. Petrovic´, N. Lajçi: Corros. Sci., 53(2011), 2176.
[33] L. Freire , M. J. Carmezim, M. G. S. Ferreira, M. F. Montemor: Electrochim. Acta., 56(2011), 5280.
[34] A. Fattah-alhosseini, H. Farahani, O. Imantalab: Int. J. ISSI., 9(2014), 19.